IEEE Access
Multidisciplinary | Rapid Review | Open Access Journal

Received 20 June 2024, accepted 27 June 2024, date of publication 9 July 2024, date of current version 19 July 2024.

Digital Object Identifier 10.1109/ACCESS.2024.3425487

RESEARCH ARTICLE

Electric Vehicle Traction System Performance Enhancement Using a High-Gain Adaptive Controller

SARAH ADNAN ALBARRI[1], AHMED KHALIL[2], SHAYOK MUKHOPADHYAY[3,4], (Senior Member, IEEE), AND HABIBUR REHMAN[1], (Member, IEEE)

[1]Department of Electrical Engineering, American University of Sharjah, Sharjah, United Arab Emirates
[2]Department of Mechanical Engineering, Texas A&M University, College Station, TX 77843, USA
[3]Department of Electrical & Computer Engineering and Computer Science, University of New Haven, West Haven, CT 06516, USA
[4]Computer Science Department, University of New Haven, West Haven, CT 06516, USA

Corresponding author: Habibur Rehman (rhabib@aus.edu)

This work was supported in part by the Open Access Program from American University of Sharjah, and in part by the Faculty Research Grant FRG22-C-E09.

ABSTRACT Electric vehicle traction systems often incorporate a field-oriented induction motor drive system with a proportional-integral (PI) speed controller having fixed gains. However, under external disturbances and parameters variation, the speed regulator performance may degrade. This work proposes solutions for tuning the PI gains of the speed regulator by using a high-gain adaptive controller, which automatically adjusts the PI controller gains based on the motor speed tracking error. To overcome gains drift caused by sensor noise, potentially leading to instability, modifications like the sigma, dead-zone, and epsilon method are applied to the adaptive law. Preliminary simulations and experimental results show that the epsilon modification-based high-gain controller outperforms the sigma and dead zone modifications for the induction motor drive system. Therefore, rigorous experimental validation of the epsilon-modified high-gain controller on an indirect field-oriented induction motor drive system is demonstrated for the following cases: square wave speed reference tracking, external disturbance rejection, detuning, field weakening, as well as different initial conditions for gains. Finally, the controller's performance is also investigated on a prototype electric vehicle (EV) traction system that consists of a 2.2 KW induction motor powered by a 400V, 6.6 A.h Li-ion battery bank. The experimental results on the prototype EV traction system validate a better speed tracking performance as compared to the fixed gains PI controller while requiring almost the same amount of current.

INDEX TERMS Electric vehicle, induction motor drive, speed regulation, indirect field orientation, high-gain adaptive controller.

I. INTRODUCTION

A. LITERATURE REVIEW

Proportional-Integral (PI) controllers are popular for speed regulation of an Indirect Field-Oriented (IFO) induction motor drive system [1]. PI gains are tuned using different techniques to provide an adequate speed response. In [2], a detailed comparison is presented among PI tuning techniques; namely, trial-error (TE-PI), Cohen-Coon (CC-PI), and Ziegler-Nichols (ZN-PI). However, speed regulation with fixed PI gains degrades under disturbances such as motor loading and motor parameters variations like, rotor resistance variations. Therefore, adaptive PI gain tuning has been investigated, with recent advancements exploring predictive strategies [3] and the application of neural networks [4]. Gain scheduling, a form of adaptive control, pre-sets different PI gains for known motor operating regions. However, this strategy is insufficient when dealing with numerous unpredictable combinations of external loading, speed references, and the difficulty of capturing the nonlinearity of the plant [5].

The associate editor coordinating the review of this manuscript and approving it for publication was Pinjia Zhang.

Therefore, fuzzy-logic and neural networks are used [6], [7], [8] for online gains scheduling. Furthermore, in [9], a fuzzy logic-based algorithm with a Genetic Algorithm (GA) based optimization routine adaptively tunes the PI gains for an induction motor drive system. An online identification method for the rotational moment of inertia is used as input to a neural network in [10]. Offline training is performed on this neural network so that it outputs the proper PI controller gains [10]. However, the application of these controllers is complex as a fuzzy controller requires setting up membership functions, and a neural network requires choosing hidden layers, number of neurons, and subsequently gathering a lot of experimental data for training the developed neural network.

Non-identifier-based rules, which have gained prominence due to their reduced need for extensive data [11], can compute PI controller gains without computing, estimating, or observing plant parameters [12]. In [13], self-tuning laws for PI gains employ the error magnitude and the direction of the change of the controller output with respect to controller input. Novel auto-tuning algorithms for PI gains have been developed [14], [15]. PI gains are validated through simple root-locus analysis [13]. In [16], the authors employ a particle swarm optimization (PSO) algorithm to tune the various PI controllers presented. An automated quantitative feedback theory (QFT)-based PI tuning method is demonstrated by [17] to highlight the superiority of the proposed PI tuning method over conventional tuning. A novel Field Oriented Control (FOC) vector structure, for a six-phase induction motor drive is presented by [18]. This structure integrates a PI controller tuned with a radial basis function neural network (RBF-NN) along with sliding mode (SM) nonlinear control.

A high-gain adaptation rule consists of adaptation and feedback laws [12]. The adaptation law uses an error signal to compute PI gains; these gains are used to generate the controller command signal in the feedback law [12]. High-gain adaptation techniques are utilized in many applications [19]-[20]. In [19] a high-gain controller is used to develop an underactuated underwater quadcopter-like vehicle. In [21], a high-gain controller tunes the controller's k_p and k_i gains for a four-wheeled mobile robot. A magnetic levitation system [20] uses a high gain law to tune the PI gains of a controller, whose output is passed through a first-order filter.

Application of the high-gain adaptive law tuning method on an IFO induction motor drive can suffer from stability problems. Adaptive gains in a PI controller may drift and not converge to a specific value in the presence of noise [12]. To overcome such issues due to gain drifting, several basic modifications are proposed for high-gain adaptation such as sigma [22], dead-zone also known as λ-tracking [23], epsilon [24], and optimal [25] control based modifications. Further adjustments to these modifications are made in [26] and [27] to ensure better stability and transient response. Various results in the literature also suggest that further research is required to enhance the stability and performance of such controllers [28]. A survey of the available literature shows that a study on the effects of high-gain adaptation to tune PI controller gains for an IFO induction motor, is not yet performed.

Modified high-gain controllers have the potential to outperform fixed PI gain controllers and, at the same time, have a simpler implementation than [6], [27], [29], and [30]. Additionally, the high-gain, modified controllers have demonstrated their potential in various applications. For example, in the dynamics of autonomous vehicles, an optimal control-based approach has been adopted for effective regulation [31]. Therefore, this work explores the potential of an adaptive PI controller using gain management modifications inspired by high gain adaptive controllers, on an induction motor driven EV traction system.

B. CONTRIBUTIONS OF PROPOSED WORK

The main contributions and novelty of the paper are summarized as follows:

- A comprehensive analysis of sigma, dead-zone, and epsilon-modified high-gain adaptive PI controllers on induction motor systems is presented, by incorporating such modifications in both simulation and experimentation.
- Simulations indicate that the epsilon-modified high-gain controller significantly outperforms the others, providing enhanced speed tracking and adaptive gain control under various input conditions.
- Experimental assessments validate the robustness and versatility of the epsilon-modified controller, with tests covering real-world operational challenges such as disturbance rejection and field weakening.
- The epsilon-modified controller has been implemented in a prototype electric vehicle traction system, demonstrating improved optimization of battery usage and overall drive performance.

In this study, a first-of-its-kind comprehensive investigation of sigma, dead-zone, and epsilon-modified high-gain adaptive PI controllers is carried out on an induction motor drive system, both in simulation and experimental setups. These high-gain modification schemes are first simulated under step reference input conditions at the motor-rated speed, with detailed comparative analysis of the speed tracking, torque commanded, current profile, k_p, and k_i gain adaptation for each scheme.

Simulations showed that among these modification strategies, the epsilon-modified high-gain controller significantly outperforms its counterparts. Therefore, an in-depth experimental assessment of this controller was conducted, where both step and square wave speed references were applied. While these modifications have been previously studied with advanced adaptive controllers, this study marks the first instance of such analysis being applied to simple adaptive PI controllers.

Further, to make this controller suitable for various operational regimes, we introduce an innovative exploration of different initial gain values upon gain resetting due

to changes in operating conditions. The effects of these varied initial conditions and resetting values are meticulously observed and compared.

The epsilon-modified high-gain adaptive controller is further tested for motor operation under low-speed tracking, disturbance rejection, detuning, and in the field weakening region. To underscore the superiority of our proposed controller, its performance is contrasted against that of a conventional fixed gains PI controller. Unlike traditional PI controllers that rely on fixed gains, the proposed controller continually fine-tunes the gains, offering an adaptive advantage that significantly enhances speed regulation performance.

Lastly, this study extends its examination to real-world applications, by applying the epsilon-modified high-gain adaptive PI controller to a prototype electric vehicle traction system. The induction motor drive system is powered using a 400V, 6.6 A.h Li-ion battery bank. A comprehensive experimental study is conducted to understand the impact of PI gain adaptation using epsilon-modified high-gain on the battery current, state of charge, voltage drop, speed tracking, and torque command current. To the best of authors' knowledge, this is the first study to analyze the impact of such an adaptive PI controller, and the gain adaptation techniques on a prototype electric vehicle traction system, offering insights for potential practical applications.

II. ELECTRICAL VEHICLE INDUCTION MOTOR DRIVE SYSTEM

A. DYNAMIC MODELING OF INDUCTION MACHINE

Induction motors are widely used in the industry because of their reliability, robustness, low cost, and self-starting behavior. It is a singly-excited machine, meaning that the power is supplied to the stator circuit only [32], and then voltage is *induced* in the rotor circuit, hence the name induction motor. Induction motors are also called asynchronous motors because the stator magnetic field speed, or the synchronous speed, ω_e, is not synchronized with the motor rotor circuit speed, ω_r [32]. The stator magnetic field speed, ω_e, is defined as in Equation (1).

$$\omega_e = \frac{4\pi f_{se}}{p} \tag{1}$$

where f_{se} is the applied electrical system frequency in hertz, and p is the motor's number of poles.

Writing the dynamic equations of an induction motor in the stationary frame of reference is a tedious task as six voltages and currents should be accounted for [33]. Nonetheless, three-phase quantities of induction motors are mostly represented using a two-axis synchronously rotating frame of reference known as the direct-quadrature, $dq-$frame. This two-axis representation allows the induction motor to be modeled and later controlled like a DC motor [33]. The $dq-$reference frame represents different rotor and stator quantities, like voltages, currents, and fluxes, in one rotating reference. The dynamic equations of an induction motor in the synchronously rotating $dq-$reference frame are often used and are shown in Equations (2) - (6) [33].

$$\frac{di_{sd}}{dt} = -\left(\frac{R_s}{\sigma L_s} + \frac{1-\sigma}{\sigma \tau_r}\right) i_{sd} + \omega_e i_{sq} + \frac{L_m}{\sigma L_s L_r \tau_r}\phi_{rd} + \frac{L_m \omega_r}{\sigma L_s L_r}\phi_{rq} + \frac{1}{\sigma L_s} V_{sd} \tag{2}$$

$$\frac{di_{sq}}{dt} = -\left(\frac{R_s}{\sigma L_s} - \omega_e i_{sd} + \frac{1-\sigma}{\sigma \tau_r}\right) i_{sq} - \frac{L_m \omega_r}{\sigma L_s L_r}\phi_{rd} + \frac{Lm}{\sigma L_s L_r \tau_r}\phi_{rq} + \frac{1}{\sigma L_s} V_{sq} \tag{3}$$

$$\frac{d\phi_{rd}}{dt} = \frac{L_m}{\tau_r} i_{sd} - \frac{1}{\tau_r}\phi_{rd} + (\omega_e - \omega_r)\phi_{rq} \tag{4}$$

$$\frac{d\phi_{rq}}{dt} = \frac{L_m}{\tau_r} i_{sq} - (\omega_e - \omega_r)\phi_{rd} - \frac{1}{\tau_r}\phi_{rq} \tag{5}$$

$$\frac{d\omega_r}{dt} = \frac{3p^2 L_m}{2JL_r}(i_{sq}\phi_{rd} - i_{sd}\phi_{rq}) - \frac{f_c \omega_r}{J} - \frac{p}{J} T_{load} \tag{6}$$

The dispersion coefficient, σ, is computed as in Equation (7),

$$\sigma = 1 - \frac{{L_m}^2}{L_r L_s} \tag{7}$$

where L_m, L_r, L_s are the mutual, rotor and stator inductances, R_r and R_s are the rotor and stator resistances, respectively. The rotor time constant is τ_r, load torque is T_{load} and the friction coefficient is f_c. Equations (2)- (6) demonstrate the nonlinearity of an induction motor, as the state variables are multiplied by one another. This nonlinearity creates challenges in controlling the induction motor outputs i.e. speed seen in Equation (6) and torque seen in Equation (8).

$$T_e = \frac{3pL_m}{2L_r}(\phi_{rd} i_{sq} - \phi_{rq} i_{sd}) \tag{8}$$

One method to eliminate the dependency of the state variables on one another so that speed and torque can be directly and linearly controlled is known as Field Oriented Control (FOC).

B. FIELD ORIENTED CONTROL OF INDUCTION MOTOR

An indirect field-oriented induction motor drive system (shown in Figure 1) is one of the most widely adopted techniques for electric vehicle traction systems. The Field Oriented Control (FOC) technique utilizes the rotor's position along with two-phase currents to produce a torque control signal. Rotor flux-oriented FOC is achieved by controlling the three-phase stator currents so that the rotor field is forced to align along the $d-$axis. Aligning the rotor flux on the $d-$axis decouples the flux and speed. Therefore, $d-$axis current is used to control the flux, and the $q-$axis current is used to control the torque. The decoupling of the $d-$axis and $q-$axis currents, or the flux and torque currents, emulates the performance of a DC motor and allows the implementation of DC motor control techniques, such as PI controller, on the induction motor. The induction motor flux is established by i^*_{sd}, later the torque is controlled by i^*_{sq}. This is analogous to establishing the flux using field current in DC motors, then controlling the torque by armature current. Conventionally,

the speed regulator shown in Figure 1 is implemented using a PI controller. However, this work attempts to improve the speed regulator performance using a PI controller whose gains are adaptively tuned using high-gain techniques and associated gain modification schemes. Therefore, the background discussion about high-gain adaptive controllers is included in the following section.

The equations aligning the rotor flux on the $d-$axis are shown in Equation (9)- (10),

$$\phi_{rq} = \frac{d\phi_{rq}}{dt} = 0 \tag{9}$$

$$\phi_{rd} = \phi_r = k \tag{10}$$

where k is a constant. Combining Equations (9) and (10) with Equation (6) and Equation (8) results in FOC torque and slip expressions in Equations (11) and (12), respectively.

$$T_e = \frac{3pL_m}{2L_r}\phi_{rd} i_{sq} \tag{11}$$

$$\omega_{sl} = \frac{L_m i_{sq}}{\tau_r \phi_{rd}} \tag{12}$$

The slip calculator shown in Figure 1 produces the desired slip given by Equation (12). This slip is the necessary and sufficient condition to guarantee the decoupled control of flux and torque of the induction machine.

III. HIGH GAIN ADAPTATION SCHEMES FOR PI CONTROLLER

If the motor drive system PI gains for the speed regulator are kept constant, the drive system performance degrades with change in the motor operating conditions. As a solution, this work implements a high-gain adaptation technique that automatically adjusts the gains based on the motor speed tracking error. A simplified schematic of the proposed adaptive PI controller configuration is shown in Figure 2. However, when high-gain adaptive PI tuning is utilized, instability occurs when this controller is tested on an induction motor. This is because the high-gain adaptive PI gains keep increasing boundlessly under external disturbances and encoder noise, thus making the system unstable. To overcome this instability, sigma, dead-zone, and epsilon modifications are applied to the high-gain adaptive law. The PI controller gains are adapted using the proposed sigma, dead-zone, and epsilon high-gain adaptive modification techniques to adjust the torque command current, i_{sq}. The sigma, dead-zone, and epsilon modifications are described in sections III-A, III-B, and III-C.

The speed error signal, $e(t)$, is defined in Equation (13), where ω_{ref} is the reference speed and ω_r is the measured motor speed. Depending on the error signal, the high-gain adaptation formula is used to derive the PI gains: i.e. proportional, k_p, and integral, k_i gains. The k_p and k_i gains are computed using Equation (14) and Equation (15), respectively.

$$e(t) = \omega_{ref} - \omega_r(t) \tag{13}$$

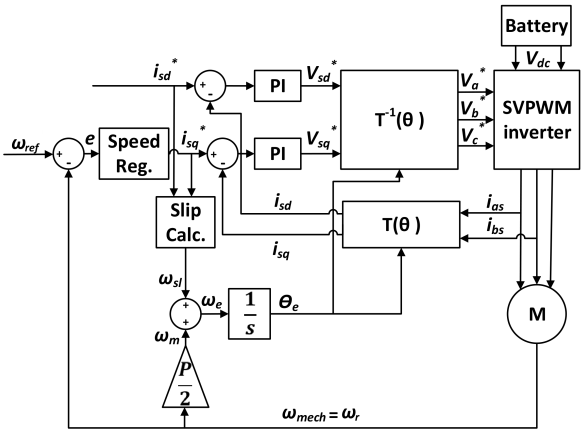

FIGURE 1. Indirect field oriented control block diagram for induction motor.

$$\dot{k}_p(t) = \mu_a e^2(t) \tag{14}$$

$$\dot{k}_i(t) = \mu_b e^2(t) \tag{15}$$

μ_a and μ_b are user-defined positive constants that determine the weight by which the error squared signal impacts the rate of change of the k_p and k_i gains, respectively. The block diagram for high-gain adaptive control to produce adaptive PI gains is shown in Figure 3.

Equations (14) and (15) and Figure 3 demonstrate that if an error signal is present, then the gains increase boundlessly. In the IFOC of an induction motor, the error signal is present as speed references and motor loading keeps changing. Moreover, even if the motor operates at a constant speed with a constant loading, the motor shaft encoder noise contributes to creating a non-zero error signal. Therefore, a standard high-gain adaptive PI-based controller is prone to instability. Thus modifications are desired which are presented in subsections III-A, III-B, and III-C. Stability analysis of these gains is not the main focus of this work. Brief comments are presented in the Appendix A related to stability of the gains when the modification schemes mentioned in this paper are used.

A. SIGMA MODIFICATION FOR GAINS ADAPTATION OF PI CONTROLLER

To overcome the boundless increase of k_p and k_i, sigma modification [22] adds a damping term that limits the gains increase as shown in Equations (16)- (17) where σ_a to σ_d are predefined positive constants.

$$\dot{k}_p(t) = \sigma_a e^2(t) - \sigma_b k_p(t), k_p(t) \geq 0 \tag{16}$$

$$\dot{k}_i(t) = \sigma_c e^2(t) - \sigma_d k_i(t), k_i(t) \geq 0 \tag{17}$$

The damping factors $\sigma_b k_p(t)$ and $\sigma_d k_i(t)$ in Equations (16) and (17) reduce the gains rate of change depending on the values of the gains. In sigma modification, the values of the gains converge to steady-state solutions [22]. However, the gains' convergence does not necessarily cause the speed error to converge to zero. The reason can be illustrated by noting that in Equations (16)- (17), when the error signal has

a large magnitude, the $e^2(t)$ terms dominate, thus the gains increase. The increase in k_p and k_i causes the motor speed, n_m, to increase and become closer to the reference speed, n_{ref}. As the error signal decreases, the damping terms become prominent and start to decrease the gain thus the motor speed decreases. As the motor speed tracking error increases, the $e^2(t)$ terms dominate again, and so on. The block diagram of the sigma modification gain adaptation is shown in Figure 4.

B. DEAD-ZONE MODIFICATION FOR GAINS ADAPTATION OF PI CONTROLLER

A straightforward solution to the issues mentioned above related to sigma modification, is to stop gain adaptation as soon as the speed error is within a reasonable predefined bound, λ. Stopping gain adaptation prevents the gains from changing as noted in sigma modification. This method is known as dead-zone or $\lambda-$modification, and it is defined in Equations (18) and (19) for k_p and k_i, respectively.

Variables α_{a-d} are positive predefined constants. The gain adaptation technique shown in the first lines in Equations(18) and (19) is the same as sigma modification Equations (16) and (17). However, the second line of Equations(18) and (19) is what defines dead-zone modification. The additional lines state that when the error magnitude reaches or becomes lesser than a user-defined limit λ, the gains rate of change is set to zero thus the gains hold their current values without any further change.

Although, theoretically, the speed tracking error converges to zero and k_p and k_i gains converge to a specific value, dead-zone modification has its own limitations. First, dead-zone adaptation might stop during transients in the motor speed response. Therefore, the adapted gains could be either too high or too low. Second, the user-defined constant λ should be chosen for the full motor speed range. This is challenging because the motor speed range is relatively large and the speed tracking performance varies for different speed ranges. Speed tracking is better for high speeds compared to low-speed tracking.

$$\dot{k}_p(t) = \begin{cases} \alpha_a e^2(t) - \alpha_b k_p(t), & |e(t)| \geq \lambda \\ 0, & |e(t)| < \lambda \end{cases} \tag{18}$$

$$\dot{k}_i(t) = \begin{cases} \alpha_c e^2(t) - \alpha_d k_i(t), & |e(t)| \geq \lambda \\ 0, & |e(t)| < \lambda \end{cases} \tag{19}$$

Also $k_p(t), k_i(t) \geq 0$ in both Equations(18) and (19).

C. EPSILON MODIFICATION FOR GAINS ADAPTATION OF PI CONTROLLER

A solution to the sigma and dead-zone modification gain adaptation limitations is known as epsilon modification, shown in Equations (20) and (21), where ϵ_a to ϵ_d are positive predefined constants.

$$\dot{k}_p(t) = \epsilon_a e^2(t) - \epsilon_b k_p(t)|e(t)|, k_p(t) \geq 0 \tag{20}$$

$$\dot{k}_i(t) = \epsilon_c e^2(t) - \epsilon_d k_i(t)|e(t)|, k_i(t) \geq 0 \tag{21}$$

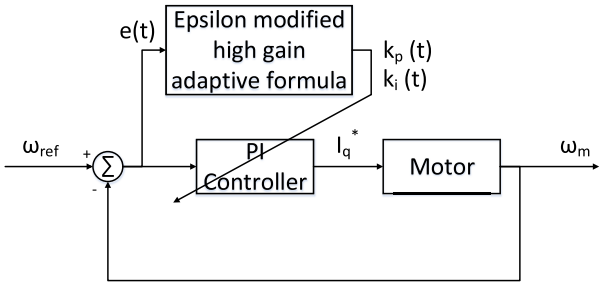

FIGURE 2. Proposed adaptive gains PI controller schematic.

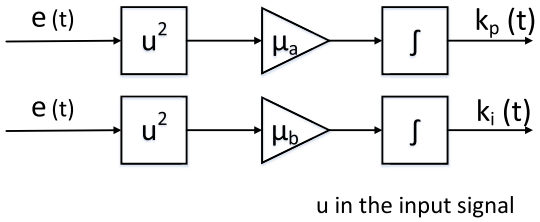

FIGURE 3. The k_p and k_i adaptation using high-gain block diagram.

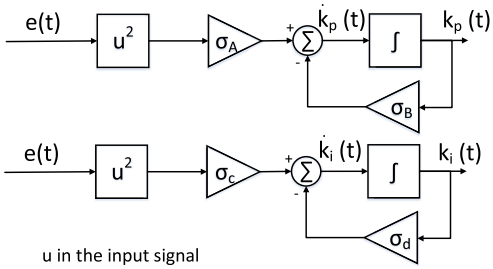

FIGURE 4. Sigma modification block diagram.

This modification works as follows; when the error magnitude is large, $\epsilon_a e^2(t)$ and $\epsilon_c e^2(t)$ terms dominate and cause the gains to increase. Increased gains reduce the error, therefore, the damping terms $\epsilon_b k_p(t)|e(t)|$ and $\epsilon_d k_i(t)|e(t)|$ decrease the values of the gains in proportion to the error magnitude. Finally, when motor speed converges to the reference speed, gain adaptation stops. The block diagram of the epsilon modification gain adaptation is shown in Figure 5.

The k_p and k_i gains computed by these high-gain modifications are used to generate the control command, $u(t)$. The control command for IFOC induction motor represents the torque command current, i^*_{sq}. Therefore, $u(t)$ is limited by an upper $i^*_{sq,max}$ and lower $i^*_{sq,min}$ bounds, as demonstrated in Equation (22). Also note that the k_p, k_i gains must be non-negative, this can be easily ensured by setting a lower bound saturation limit of zero when any of the proposed high-gain adaptation schemes are used.

$$u(t) = i^*_{sq} = k_p(t)e(t) + k_i(t)\int e(t)dt, \quad \text{where } i^*_{sq,min} < u(t) < i^*_{sq,max} \tag{22}$$

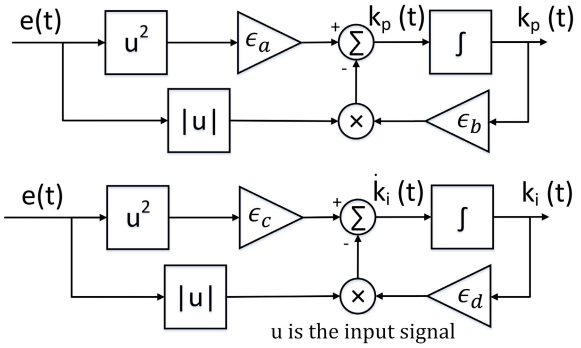

FIGURE 5. Epsilon modification block diagram.

TABLE 1. Sigma, dead-zone, & epsilon modification constants for step simulation.

Sigma & Dead-zone		Epsilon	
Quantity	Values	Quantity	Values
σ_a, α_a	35×10^{-5}	ϵ_a	22×10^{-5}
σ_b, α_b	0.1	ϵ_b	0.1×10^{-5}
σ_c, α_c	18×10^{-5}	ϵ_c	23×10^{-5}
σ_d, α_d	0.1	ϵ_d	0.1×10^{-5}

D. PERFORMANCE METRICS

Metrics that evaluate the speed tracking error signal are integral squared error (ISE), integral absolute error (IAE), and integral time absolute error (ITAE). The equations for which are shown in Equations (23) - (25), respectively.

$$IAE = \int |e(t)|dt \tag{23}$$

$$ISE = \int e^2(t)dt \tag{24}$$

$$ITAE = \int te(t)dt \tag{25}$$

The ISE amplifies higher magnitude errors as noted in the $e^2(t)$ term. Therefore, overshoot and undershoot effects are more prominent. IAE reports the integral of the error signal, thus, a response with a large overshoot and small settling time might score the same as a response with a small overshoot and large settling time. ITAE accounts for the duration and magnitude of the error signal. The mean absolute value of i^*_{sq} quantifies the quadrature current i^*_{sq} magnitude commanded by each controller. This is shown in Equation (26), where N is the number of commanded quadrature current samples.

$$i^*_{sq}avg. = \frac{1}{N}\sum_{k=1}^{N} |i^*_{sq}[k]| \tag{26}$$

IV. SIMULATION STUDY OF HIGH-GAIN ADAPTIVE CONTROL TECHNIQUES FOR IM DRIVE SYSTEM

Simulation results are obtained for sigma, dead-zone, and epsilon-modified high-gain adaptation schemes for tuning PI controller gains. The total simulation duration is 10 seconds; in the first five seconds a step reference of the rated speed 1500 rpm is applied to the IFO induction motor drive system.

TABLE 2. Simulation evaluation for sigma, dead-zone, and epsilon.

Metric	Sigma	dead-zone	Epsilon
IAE	29.18	18.53	19.49
ISE	813.0	825.5	849.7
ITAE	129.88	59.75	46.8
i^*_{sq} $avg.$ (A)	0.8894	0.8905	0.8910

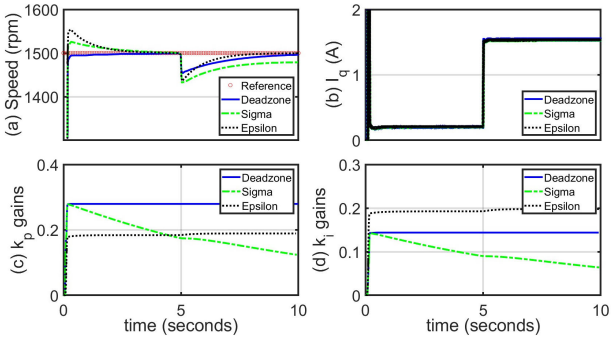

FIGURE 6. Simulation (a) Speed tracking, (b) I_{sq}, (c) k_p gains, (d) k_i gains.

At the fifth second, the motor is loaded with 2 N.m. The load is applied to investigate the performance of each gain adaptation technique to disturbance rejection. The constants σ_a to σ_d, α_a to α_d and ϵ_a to ϵ_d used in Equations (16)- (21) are shown in Table 1. The speed tracking and commanded quadrature current along with the gain adaptations over time for each technique are plotted in Figure 6. The overall performance evaluation for the three high-gain modifications is summarized in Table 2. All three modifications require about the same torque command current. The maximum quadrature current consumption difference occurs between sigma and epsilon modifications, it is equal to 0.0016 A with a percentage difference of 0.18%. After the load application, sigma modification speed tracking has a steady-state error which is emphasized by having the largest IAE and ITAE values. In Figure 6, the k_p and k_i adaptations for sigma modification are decreasing until the gains reach steady-state values. The speed tracking performance of the dead-zone modification is relatively the best as indicated by the lowest IAE and ISE values. However, as can be seen in Figure 6, the dead-zone modification stopped k_p, and k_i gains adaptation directly after the speed step input is applied. The reason is that the λ for dead-zone adaptation seen in Equations (18) and (19) is set to 90 rpm. The value of λ is found based on the trial-and-error method. The value of λ should be large enough to prevent the gains from decreasing, based on Equations (18 and 19), as a small speed-tracking error reduces the gains. At the same time, the value of λ should be small enough to obtain a proper speed transient response. As for epsilon modification, the gains converged to a value after a speed step input is applied. When the load is applied at the fifth second, the k_p and k_i values adapt by increasing. In this modification, gains increase to adapt to changes whenever an error is present. As for the speed tracking performance for epsilon modification, it has a superior ITAE

which can be noted in Figure 6 as the error converges faster. Epsilon modification IAE and ISE values are comparable to the dead-zone modification with percentage differences of 5.05% and 2.89% respectively. Therefore, based on the simulation investigation, Epsilon modification is selected for further experimental trials. It does not require an additional tuning parameter (such as λ in dead-zone modification) and has a lower steady-state error when compared with sigma modification.

V. PROTOTYPE IM DRIVE AND OVERALL EV TRACTION SYSTEM

The IFO drive system experimental setup consists of a DC power source, a three-phase power inverter, a Siemens induction motor, current sensors, a dSPACE data acquisition board, and a computer. The power inverter converts a fixed DC bus voltage which is coming either from an AC/DC converter or from a battery bank to a three-phase AC signal. The induction motor current and speed are measured using LEM current sensors and an encoder. The overall prototype EV traction system is shown in Figure 7.

A. BATTERY BANK AND THREE-PHASE POWER INVERTER

Lithium-ion (Li-ion) batteries are extensively researched and used in battery-powered electric vehicles (BEVs) [34]. The reasons for Li-ion batteries' popularity are superior performance in terms of high energy and power density, negligible memory effect, and low self-discharge rate [35].

State of charge (SOC), state of health (SOH) are some evaluation metrics of a battery's state [35]. SOC measures the amount of charge available in a battery compared to the battery's full charge capacity at the beginning of a discharge cycle. It informs the user of the remaining battery runtime and enables protection from over-discharging and also allows fault detection [34], [35]. The simplest and most commonly used method to estimate SOC is through Coulomb counting because it is relatively easy to implement and has a simple structure, seen in Equation (27).

$$SOC(t) = SOC(t_0) - \frac{1}{C_c}\int_{t_0}^{t} i(t)dt \tag{27}$$

In Equation(27), $SOC(t_0)$ is the initial value of SOC and C_c is the battery capacity factor in $A.s$. The current $i(t)$ is defined to be positive if the battery is discharging, and negative if the battery is charging. As can be seen from Equation (27), SOC computation depends heavily on the accuracy of the initial value of $SOC(t_0)$ and the accuracy of the method used to read or compute the current. A small error in current readings can accumulate over time due to the integration effect. Therefore it is advised to use accurate sensors when this method is used to estimate SOC. The details of the individual battery and the overall battery bank are shown in Table 5.

The three-phase power inverter, seen in Figure 7, converts the DC voltage into an AC voltage. The inverter used consists of six IGBTs (Insulated-Gate Bipolar Transistors), two in each leg. An IGBT three-phase inverter is used because it is compact in size, operates with a switching frequency of up to 20 kHz, and contains many protective systems such as overvoltage, overcurrent, and overtemperature protection. IGBTs are semiconductor devices that combine the simplicity of the gate drive of a metal-oxide-semiconductor field-effect transistor (MOSFET), and the high current-withstanding abilities of the Bipolar Junction Transistor (BJT). Because of their high current handling and voltage-blocking capabilities, IGBTs are used in applications that require medium to high power.

TABLE 3. Siemens induction motor specifications.

Model Name	1LE1001-1AB42
Rated power	2.2 kW
Rated voltage	400 V
Rated current	4.65 A
Rated speed	1455rpm
Rated torque	14.4 N.m
Rated frequency	50 Hz
Power factor	0.81
Poles	2
Stator resistance (R_s)	3.24Ω
Stator inductance (L_s)	0.0458H
Rotor resistance (R_r)	1.31Ω
Rotor inductance (L_r)	0.0102H

TABLE 4. Current sensor specifications.

Model Name	Max. Current	V_{supply}	Resistance
LEM LA-25 NP	25 A	±15 V	220Ω

TABLE 5. Battery bank specifications.

Total number of batteries	16
Bank capacity	6600mAh
Nominal voltage of each battery	22.2 V
Maximum voltage of each battery	25.2 V
Maximum bank voltage	403.2 V

B. INDUCTION MOTOR, CURRENT SENSOR, ENCODER, AND DSPACE 1103 BOARD

The induction motor to be tested is a three-phase squirrel cage motor shown in Figure 7. The specifications of this motor are noted in Table 3. Two current sensors, connected to two phases, are used to operate an induction motor with IFOC. These measured phase currents are then transformed into $dq-$currents, as shown in Figure 1. Therefore, the control of flux and torque can be established. The specifications of the LEM LA-25 NP current sensors are shown in Table 4.

The encoder resolution is 1024 pulses per revolution and it is mounted at the back of the motor. The current sensor and encoder readings are processed by the dSPACE 1103 board. A dSPACE 1103 is a Digital Signal Processor (DSP) board with an A/D and D/A converter resolution of 16 bits, 16 multiplexed channels, and a quad-core AMD x86 processor. It offers fast processing and real time interface

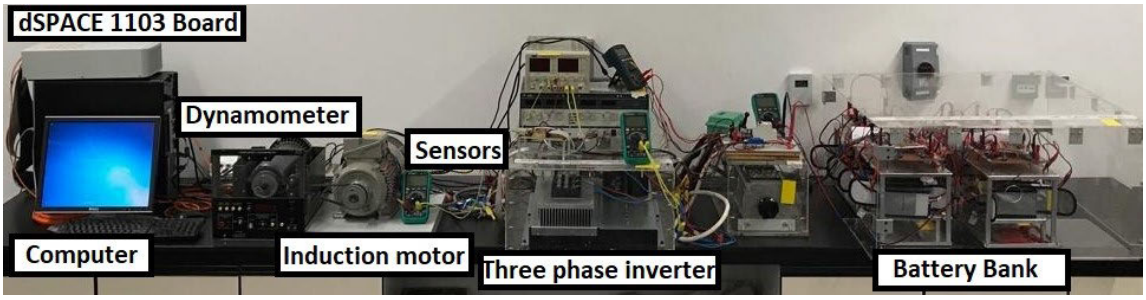

FIGURE 7. Overall experimental setup.

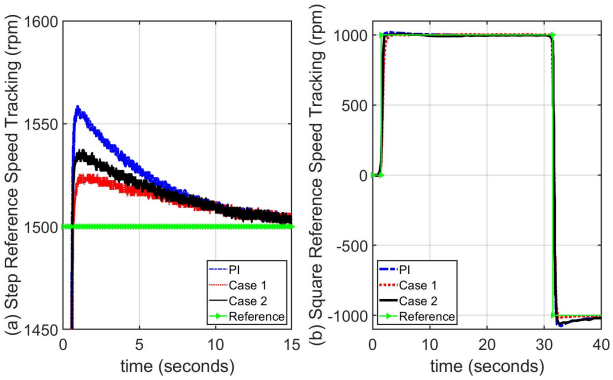

FIGURE 8. Speed step (a) and square (b) tracking for fixed gains and epsilon-modified high-gain (Case 1 and 2).

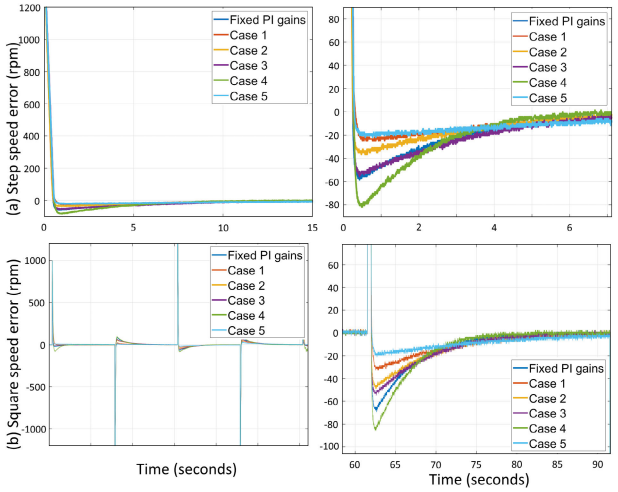

FIGURE 9. Speed step (a) and square (b) tracking error for fixed gains and epsilon-modified high-gain.

(RTI). RTI is important to process the data input and output from analog-to-digital converter (ADC), digtial-to-analog converter (DAC), and the encoder input readings. The software interfaced with the experimental setup is MATLAB Simulink 2013a. The computer on which the software is present has an Intel Xeon processor, and Windows 10, 64-bit operating system.

VI. EXPERIMENTAL RESULTS

A. PERFORMANCE EVALUATION FOR SPEED STEP & SQUARE REFERENCE TRACKING

The effect of resetting the adapted PI gains as the motor speed reference becomes zero is studied. Since these modifications are done on an adaptive PI controller, the effect of different initial values is studied. The speed tracking errors and i_{sq}^{*} averages of the fixed PI gains based controller, and the proposed adaptive PI gains based controller with the different resetting values are tabulated in Table 6. Case 1 to 5 represent different (k_p and k_i) resetting values of (0,0), (0.08, 0.013), (0.1, 0.0175), (0, 0.0175) and (0.1,0), respectively. For clarity, only two of these cases are shown in Figure 8. It can be noted that adaptation using epsilon-modified high-gain produces a better speed tracking performance and commands the same or lower i_{sq}^{*} and rms value of phase current $I_a(rms)$ compared to the conventional fixed gains PI controller. The speed tracking errors for all five cases are also shown in Figure 9.

Case 1 starts with the lowest k_p and k_i reset values, which result in a small overshoot value and a long time for the speed tracking error to converge to zero. As the reset values of k_p and k_i are increased to 0.08 and 0.013, respectively, the overshoot increases, and the time for the speed tracking error to converge to zero decreases. However, in Case 2 IAE, ISE, and ITAE are higher than Case 1. Case 3 introduces an additional increase in the k_p and k_i reset values to 0.1 and 0.0175. The speed tracking performance of this controller becomes similar to the fixed gains PI controller as noted in Figure 9. Therefore, it is concluded that any further increase in k_p and k_i reset values will not have a positive effect on controller speed tracking performance. Case 4 and Case 5 validate the effects of having the initial conditions and reset values to have either k_i value (0, 0.0175) or k_p value (0.1 0), respectively. For the (0, 0.0175) case, the highest speed overshoot is observed due to the high k_i value adaptation as seen in Figure 9. Nonetheless, the speed error converges to zero faster than any other resetting case. On the contrary, Case 5 has the lowest speed overshoot and the longest time for speed error convergence to zero. The speed error computation at a defined time enables a fair comparison of the control schemes. At the 12^{th} second, the speed tracking error magnitude for fixed gains PI controller is 5.68 rpm,

TABLE 6. Performance evaluation for fixed gains PI controller and epsilon-modified high-gain adaptive PI controller for speed step and square tracking.

Test	Metric	PI	Case 1	Case 2	Case 3	Case 4	Case 5
Step	IAE	72.67	59.64	62.04	79.01	76.25	68.75
	ISE	4.23×10^3	3.81×10^3	4.03×10^3	4.68×10^3	4.54×10^3	4.45×10^3
	ITAE	4.85×10^4	4.76×10^4	4.78×10^4	4.79×10^4	4.87×10^4	4.75×10^4
	$\%OS$	3.9	1.66	2.44	3.713	5.467	1.467
	$i^*_{sq}avg.$	0.2540	0.2476	0.2497	0.2518	0.2466	0.2487
	$I_a(\text{rms})$	0.7921	0.7241	0.7551	0.7644	0.7577	0.7608
Square	IAE	332.1	311.6	317.3	322.16	386.8	272.1
	ISE	2.58×10^3	2.47×10^3	2.51×10^3	2.56×10^3	2.78×10^3	2.465×10^3
	ITAE	3.63×10^4	3.47×10^4	3.51×10^4	3.56×10^4	4.19×10^4	3×10^4
	$i^*_{sq}avg.$	0.2178	0.2061	0.2154	0.2122	0.2132	0.2088
	$I_a(\text{rms})$	0.7721	0.7524	0.7681	0.7634	0.7613	0.7679

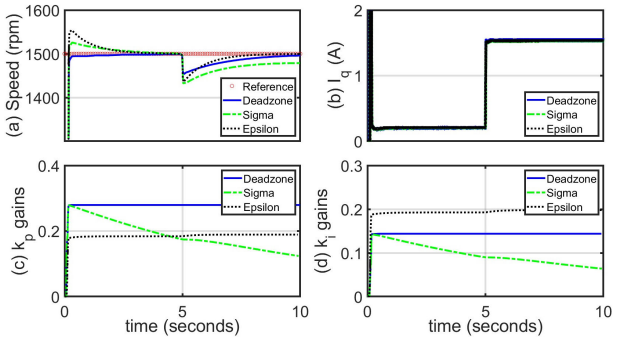

FIGURE 10. Low speed tracking (a) Speed tracking, (b) i^*_{sq}, (c) k_P gains, (d) k_I gains.

Case 1 is 7.32 rpm, Case 2 is 6.72 rpm, Case 3 is 5.67 rpm, Case 4 is 1.465 rpm, and Case 5 is 10.25 rpm. Setting the initial k_i gains gains to non-zero positive values, based on the operator's knowledge of the actual parameters, can accelerate the convergence of the k_i gains. This adjustment facilitates quicker speed-tracking error convergence. This is because a non-zero positive gain value is likely to be closer to the actual and possibly optimal gain value, as opposed to a gain of value zero. Conversely, if the initial k_i gains are set to zero, i.e. further from their optimal values, the convergence process will be slower, leading to delayed speed-tracking error convergence. This resetting process also does not require knowledge of the actual optimal gain values.

B. PERFORMANCE EVALUATION UNDER LOW SPEED TRACKING

The controller performance under low speed tracking is an important controller performance testing metric. The speed tracking and commanded quadrature current, i^*_{sq}, of the conventional fixed gains and adaptive gains based PI controller are plotted in Figure 10(a) and (b). Moreover, the gains adaptation for each technique is plotted in Figure 10(c) and (d). The performance analysis of each controller scheme for low speed tracking is presented in Table 7. Furthermore, the epsilon modification constants, shown in Equation (20) and (21), used for low speed tracking are tabulated in Table 10.

TABLE 7. Performance evaluation for low speed tracking test.

Metric	Fixed PI	Adaptive PI
$i^*_{sq}avg.(\text{A})$	0.1267	0.1050
$I_a(\text{rms})(\text{A})$	0.7003	0.6974
Upper speed limit (rpm)	109.86	112.79
Lower speed limit (rpm)	87.89	82.03
Δ Speed (rpm)	22.1	30.8

The low-speed regulation of the epsilon-modified high-gain adaptive controller is worse than that of the fixed gains PI controller. This can be seen when the speed starts oscillating around the values of 100 rpm in Figure 10(a). The epsilon modification speed tracking error oscillates between 82 and 112.8 rpm, whereas, the fixed gains PI controller speed tracking error oscillates between 87.9 and 110 rpm. The Δ speed is calculated based on these speed oscillations at the steady state value and are shown in Table 7. Nonetheless, the epsilon-modified high-gain adaptation outperforms the conventional fixed gains PI controller with lower i^*_{sq} consumption. The epsilon modification average i^*_{sq} commanded is 0.1050 A compared to 0.1267 A for fixed gains PI controller. The speed tracking steady-state is not reached for fixed gains and epsilon-modified high-gain adaptive controller as noted by the motor speed oscillating around the reference value.

C. PERFORMANCE EVALUATION UNDER DISTURBANCE REJECTION

In disturbance rejection test, as the motor operates at its rated speed of 1500 rpm, a step load disturbance of 1 N.m is added and later removed. The speed and commanded quadrature current profiles, i^*_{sq} for fixed and adaptive gains PI controllers are shown in Figures 11(a) and (b). Moreover, the PI gains are plotted in Figure 11(c) and (d). Figure 11 demonstrates that epsilon-modified high-gain adaptive PI controller outperforms fixed gains PI controller in terms of speed response to a step load while commanding almost the same amount of current. A detailed evaluation of the performance of the two controllers is presented in Table 8.

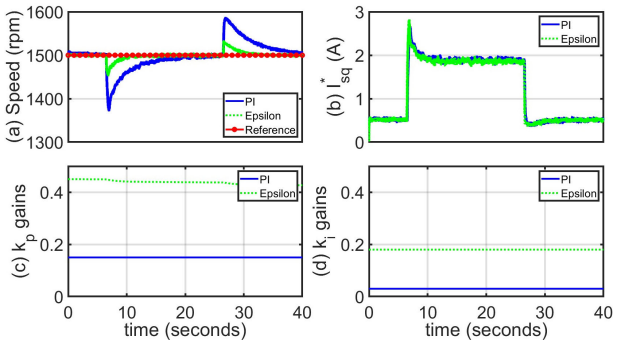

FIGURE 11. Disturbance rejection (a) Speed tracking, (b) i^*_{sq}, (c) k_p gains, (d) k_i gains.

TABLE 8. Performance evaluation for disturbance rejection test.

Metric	Fixed PI	Adaptive PI
IAE	181.13	125.4
ISE	6.36×10^3	6.33×10^3
ITAE	1.41×10^4	0.83×10^4
$i^*_{sq}avg.$	1.117	1.1015
$I_a(\text{rms})$	1.263	1.284
$\%OS$	5.76	2.146
$\%US$	8.33	3.13

The epsilon-modified high-gain adaptive PI managed to outperform the fixed gains PI controller with the same amount of average commanded quadrature current. When the 1 N.m load is added, the fixed gains controller speed decreased to 1375 rpm whereas the adaptive gains PI controller speed decreased to 1453 rpm. As for the gain adaptation in Figure 11(c) and (d), k_p and k_i gains didn't experience many changes as the speed error is small. The presence of the small error and the high-gains values cause k_p gains adaptation over time to decrease as the second term, $-\epsilon_b k_p|e(t)|$ in Equation (20) dominates. This occurs as a direct result of the choice of the ϵ_a to ϵ_d constants, seen in Table 10.

D. PERFORMANCE EVALUATION UNDER DETUNING

The speed controller testing under the detuning condition is yet another important metric for evaluating the controller performance. To perform the detuning test as the motor operates at its rated speed of 1500 rpm, the rotor time constant of 3.8 is changed to half its value, 1.9. The forceful changes in the rotor time constant are shown in Figure 12. The wrong value of the rotor time constant is fed to the IFO scheme. The resulting speed and commanded quadrature current profiles for fixed gains and adaptive gains PI controllers are shown in Figure 13(a) and (b). Moreover, the PI gains adaptation is plotted in Figures 13(c) and (d). The epsilon modification constants ϵ_a, ϵ_b, ϵ_c, and ϵ_d are are chosen as shown in Table 10. The constants for this test are chosen to prepare the epsilon-modified high-gain adaptation scheme to handle any sudden speed tracking error unrelated to the speed reference change.

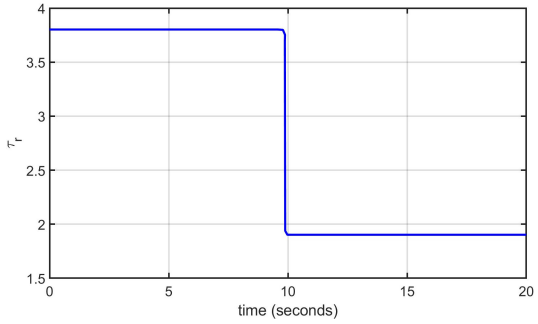

FIGURE 12. Rotor time constant for detuning test.

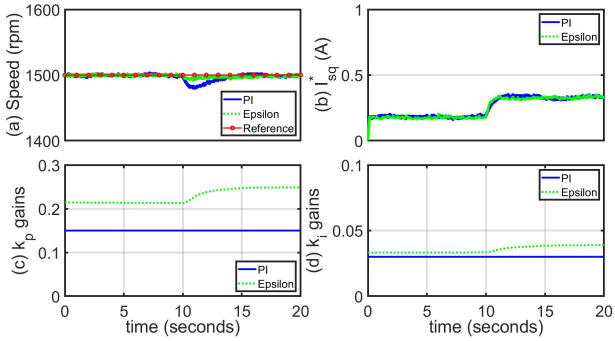

FIGURE 13. Detuning (a) Speed tracking, (b) i^*_{sq}, (c) k_p gains, (d) k_i gains.

TABLE 9. Performance evaluation for motor operation under detuning.

Metric	Fixed PI	Adaptive PI
IAE	87.57	76.71
ISE	4.79×10^3	3.89×10^3
ITAE	5.01×10^3	4.40×10^3
$i^*_{sq}avg.$	0.2694	0.2658
$I_a(\text{rms})$	0.7232	0.7303
$\%US$	1.2	0.47

The detailed evaluation for the controller's performance under detuning is presented in Table 9. The adaptive PI controller outperforms the fixed gains PI controller in terms of speed regulation noted in lower IAE, ISE, and ITAE values in detuning. Moreover, the motor speed for fixed gains PI controller decreases to 1479.5 rpm compared to 1492.7 rpm for the adaptive gains. When the motor is detuned, the adaptive k_p and k_i gains, shown in Figure 13(c) and (d), increase from 0.2128 and 0.033 to 0.2483 and 0.03857, respectively. The commanded quadrature currents for both PI controllers are somehow equivalent with 0.2694 A for the fixed gains and 0.2658 for adaptive gains PI controllers.

E. PERFORMANCE EVALUATION UNDER FIELD WEAKENING

The work presented in this paper attempts to investigate the controllers' performance under almost all kind of motor operating conditions. Therefore, the motor operation in the field weakening region is considered as well. In the field weakening region, above the motor rated speed, the motor

flux is reduced to decrease the motor back EMF because the input voltage has already reached at its rated value. The motor flux is linearly decreased by commanding a lower i_{ds}^{*} when the reference speed ω_{ref} surpasses the rated speed of 1500 rpm. Equation (28) is used to obtain i_{ds}^{*} for every speed input. Figure 14 plots i_{ds}^{*} as a function of time.

To test if the epsilon-modified high-gain adaptive PI controller can track the speed in field weakening, a step input of 600 rpm is applied followed by a linear increase in the speed till it reaches 2500 rpm. The epsilon modification constants used for the field weakening test are tabulated in Table 10. The speed tracking and quadrature current profiles are shown in Figures 15(a) and (b). Furthermore, the PI gain adaptation for each controller is shown in Figures 15(c) and (d). Both controllers are able to track reference speed commands in the field weakening region. The speed tracking performance of both controllers is almost the same as there are no abrupt changes in the speed input. However, the mean absolute commanded quadrature current by the fixed PI controller is 0.3096 A, which is higher than the epsilon-modified high-gain adaptive PI controller, 0.2981 A.

$$i_{ds}^{*} = \begin{cases} 0.90, & \omega_{ref} < 1500rpm \\ -0.0003\omega_{ref} + 1.35, & 1500 \leq \omega_{ref} \leq 2500rpm \end{cases} \tag{28}$$

VII. PERFORMANCE ASSESSMENT OF EPSILON-MODIFIED HIGH-GAIN ADAPTIVE PI CONTROLLER ON A PROTOTYPE ELECTRIC VEHICLE TRACTION SYSTEM

After rigorously testing the proposed controllers' performance under various motor operating conditions, finally the controllers are tested on the EV traction system while being powered by the 400 V Li-ion battery bank. This section presents the experimental data gathered over the duration of a NEDC drive cycle for fixed and adaptive gains PI controller on a prototype electric vehicle traction system. Subplots (a) and (c) in Figure 16 contain the speed tracking profile and subplots (b) and (d) provide the speed tracking error signal for fixed and adaptive gains PI controllers, respectively. The speed tracking error signal attains its highest overshot values at low speed tracking. It is evident that the adaptive PI gains outperforms the fixed PI gains. The speed tracking error for the adaptive gains PI controller ranges between -23.44 and 20.9 rpm. Whereas, the speed tracking error for the fixed gains PI controller ranges between -40.12 and 33.2 rpm. The adapted k_p and k_i gains are plotted in Figure 17. The gains values are reset whenever the motor reference speed is zero. The k_p gain is reset to 0.08 and the k_i is reset to 0.2. These resetting values are found by trial-and-error method; different resetting values are tried and the one with the best overall performance is chosen. The gain adaptation overshoots at low speeds due to the worse overall performance of the induction motor in low speeds. This increase in the gains value occurs when the higher speed tracking error magnitude occurs as seen in subplots (b) and (d) in Figure 16.

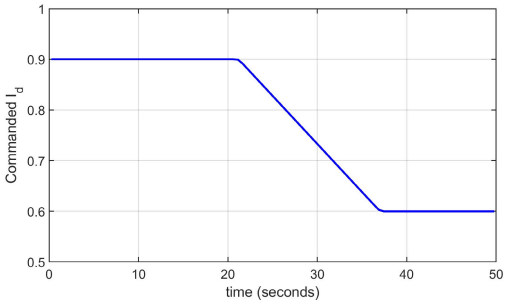

FIGURE 14. Commanded stator direct current for field weakening test.

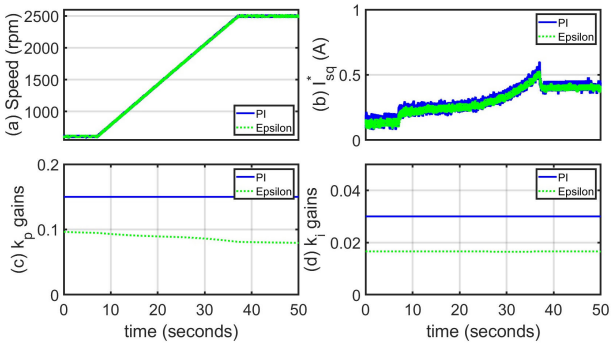

FIGURE 15. Field weakening (a) Speed tracking, (b) i_{sq}^{*}, (c) k_p gains, (d) k_i gains.

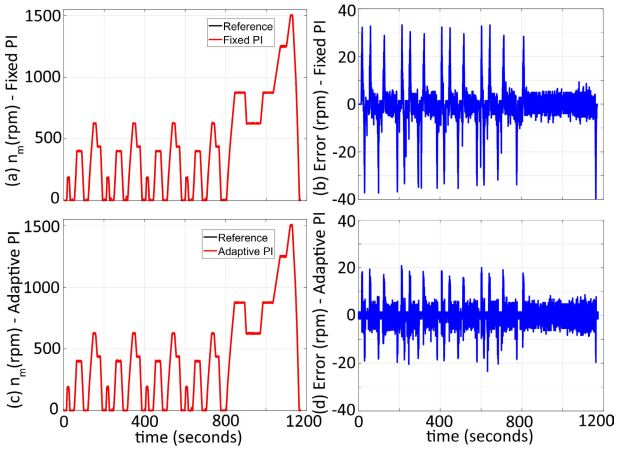

FIGURE 16. Overall speed tracking performance for fixed (a and b) and adaptive gains (c and d) PI controller for EV traction system.

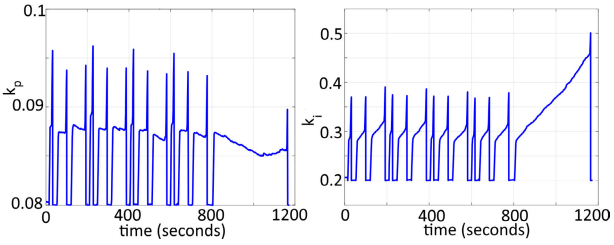

FIGURE 17. Gains adaptation for NEDC drive cycle (a) k_p and (b) k_i.

TABLE 10. The values of ϵ_a, ϵ_b, ϵ_c and ϵ_d for all experimental tests.

	ϵ_a	ϵ_b	ϵ_c	ϵ_d
Step speed tracking (Section VI-A)	4.85×10^{-5}	6.4×10^{-3}	6.23×10^{-6}	6.4×10^{-4}
Square speed tracking (Section VI-A)	2.3×10^{-5}	4.7×10^{-3}	2.3×10^{-6}	5×10^{-4}
Low speed tracking (Section VI-B)	9.7×10^{-3}	0.2	8×10^{-4}	0.2
Disturbance rejection (Section VI-C)	9.5×10^{-5}	3.5×10^{-3}	3×10^{-5}	2.5×10^{-4}
Detuning (Section VI-D)	0.08	0.07	0.0095	0.04
Field weakening (Section VI-E)	2.7×10^{-4}	1.6×10^{-2}	3×10^{-5}	2.1×10^{-2}

TABLE 11. Performance evaluation for BEV application.

Metric	Fixed PI	Adaptive PI
IAE	447.62	265.2
ISE	667.5	178.99
ITAE	2.61×10^5	1.68×10^5
$i^*_{sq}avg.$ (A)	1.033	0.9988
I_{battery} (avg.) (A)	0.3549	0.3447
$\Delta SOC(\%)$ used	2.89	2.81
Δ Voltage(V) drop	1.81	1.31

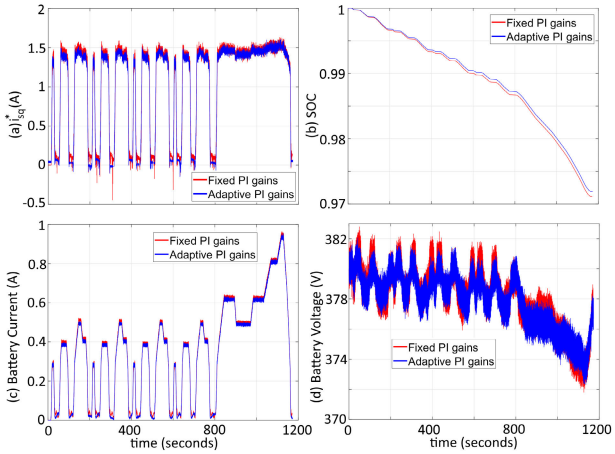

FIGURE 18. Battery (a) Quadrature Current, (b) SOC, (c) Output Current, and (d) Voltage Drop.

To further investigate the performance of the controller on an EV application, the motor control effort i^*_{sq} and the battery current are plotted in Figure 18(a), (c) respectively. The fixed gains PI controller consistently consumes higher current from the battery compared to the adaptive gains PI controller. This is also evident by the lower value of SOC reached by the fixed gains PI controller, 0.9711 compared to 0.9719 for adaptive gains PI controller. The battery output current and voltage are plotted in Figures 18(c) and (d). The battery current consumption for the fixed gains controller on average is 0.3549 A and for the adaptive gains controller is 0.3447 A. Moreover, the torque command current by the adaptive gains controller is 0.9988 A compared to 1.033 A by the fixed gains PI controller. For both controllers, the battery bank is charged to obtain a starting voltage around 380 V as observed in subplot (d) of Figure 18. However, at the end of the NEDC drive cycle the battery bank voltage is 378.19 V for fixed gains PI controller and 378.69 V for adaptive gains PI controller. Table 11 quantifies the results obtained in Figures 16-18 for adaptive gains PI controller in comparison to the fixed gains PI controller. The adaptive PI gains controller outperforms the fixed gains using the IAE, ISE, and ITAE evaluation metrics as seen in Table 11. Based on the superior performance evaluation metrics values, the conclusion drawn is that adaptive high-gain epsilon modification controller outperforms fixed gain PI controller and therefore can be employed in electric vehicle traction systems. It is also worth considering that the test shown here is only over a duration of 1200s where was for a real-life EV application, such small improvements over time have the potential to add-up to larger performance benefits and lower battery degradation.

VIII. CONCLUSION

This work implemented and evaluated the performance of sigma, dead-zone, and epsilon-modified high-gain adaptive techniques to auto-tune PI controller gains of an IFO induction motor drive system. The controllers' comparison showed that epsilon modification had superior gain adaptation performance. Therefore, the second part of the work focused on a rigorous experimental validation of the high-gain epsilon modification for PI gains adaptation applied to an IFO-based induction motor drive system. For step and square input tracking, the effect of different sets of initial conditions and resetting values is studied. It is found that using small values of initial gains and reset values for k_p and k_i such as 0.08 and 0.013 enhance the overall gain adaptation and speed tracking performance while maintaining relatively the same torque command current.

Motor operation for disturbance rejection, under detuning, and in the field weakening region is also evaluated for the epsilon-modified high-gain adaptation of PI gains. For all the performance evaluation tests, the performance of epsilon modification is compared with the performance of the conventional fixed gains PI controller. In disturbance rejection tests, the PI controller with adaptive gains outperforms the fixed gains controller in terms of speed tracking by scoring lower IAE, ISE, and ITAE. Moreover, the speed tracking enhancement occurs with a lower torque command current of the adaptive gains PI controller (1.1015 A) than the fixed gains PI controller (1.1170 A). When the motor is operated under detuning, the speed tracking of the adaptive gains PI controller and the torque command current is also found to be better than the fixed gains PI controller as noted by lower

IAE, ISE, ITAE and average commanded quadrature current values. Finally, the adaptive PI gains are also able to perform well when the motor is operating in the field weakening region.

Motivated by the overall better performance of the adaptive gains PI controller, the adaptive PI gains technique is applied to an IFO electric vehicle prototype traction system. NEDC drive cycle was used so that the PI gains adaptation is evaluated for different speed ranges. The adaptive gains PI controller is able to regulate the speed with a lesser error range of -23.44 to 20.9 rpm compared to -40.12 to 33.2 rpm for fixed gains PI controller with lower battery current consumption and torque command current. The lower battery energy consumption of the high-gain epsilon modification based adaptive controller for a short time duration NEDC drive-cycle test shows that for the case of long EV operation time; there may be significant energy savings while providing better speed tracking. Thus, overall high-gain epsilon modification based adaptive controllers have a great potential for EV traction system applications.

APPENDIX

The full-fledged stability analysis involving the gain adaptation schemes and the PI speed controller is not the focus of the current work. This work is more interested in examining the effects of using such gain modifications on a prototype EV tracking system. In the following subsections, we provide some comments related to how stability analysis may be approached.

A. COMMENTS ON STABILITY ANALYSIS FOR SIGMA MODIFICATION

The equations for gain adaptation using sigma modification can be easily morphed in the state space form $\dot{x} = Ax + Bu$, where $x = [k_p \quad k_i]^T$, $A = \begin{bmatrix} -\sigma_b & 0 \\ 0 & -\sigma_d \end{bmatrix}$, $B = [\sigma_a \quad \sigma_c]^T$, and $u = e^2$. From this, it is obvious that the system of equations in 16, 17 is a stable LTI system. As long as the error stays bounded the gains stay bounded too. If the PI controller that uses these gains drives the error e to zero, the gains converge.

B. COMMENTS ON STABILITY ANALYSIS FOR DEAD ZONE MODIFICATION

If the speed error is less than λ, then the gains do not change. On the other hand, if the error is greater than or equal to λ then the discussion exactly as in section VIII-A holds with the following equations $\dot{x} = Ax + Bu$, where $x = [k_p \quad k_i]^T$, $A = \begin{bmatrix} -\alpha_b & 0 \\ 0 & -\alpha_d \end{bmatrix}$, $B = [\alpha_a \quad \alpha_c]^T$, and $u = e^2$.

C. COMMENTS ON STABILITY ANALYSIS FOR EPSILON MODIFICATION

In equations 20, 21 let $x = [k_p \quad k_i]^T$ then consider the candidate Lyapunov function $V(x) = 1/2(x^T x) = (1/2)k_p^2 + (1/2)k_i^2$. Then the time derivative of V can be written as $\dot{V}(x) = -|e(t)|(\epsilon_b k_p^2(t) + \epsilon_d k_i^2(t)) + e^2(t)(\epsilon_a k_p(t) + \epsilon_c k_i(t))$. If the values of k_p and k_i are such that $k_p(t)^2$ is greater than $k_p(t)$ and $k_i(t)^2$ is greater than $k_i(t)$, and if the PI controller makes the $|e(t)| < 1$ then $e(t)^2 < |(e(t))|$. Further, if ϵ_b, ϵ_d are selected such that $\epsilon_b > \epsilon_a$ and $\epsilon_d > \epsilon_c$ then we have $|e(t)|(\epsilon_b k_p^2(t) + \epsilon_d k_i^2(t)) > e^2(t)(\epsilon_a k_p(t) + \epsilon_c k_i(t))$. This gives $\dot{V}(x) < 0$ which makes the gains k_p and k_i converge. Now clearly for the above to hold the gains k_p, k_i have to be non-zero, otherwise if $k_p = 0$ and $k_i = 0$ then $\dot{V}(x) = 0$. Which means the gains do not change. Based on this observation, rather than starting the gain adaptation process from $k_p = 0$ and $k_i = 0$, if the process is started such that k_p, k_i have non zero values, then it is possible that the gain convergence could be faster and thus better speed tracking performance would be obtained faster than the case of initializing the gains from zero.

DISCLAIMER

This article represents the opinions of the author(s) and does not mean to represent the position or opinions of the American University of Sharjah.

REFERENCES

[1] P. Sarkar, A. Hazra, and A. Mondal, "A unified approach for PI controller design in delta domain for indirect field-oriented control of induction motor drive," *J. Eng. Res.*, vol. 8, no. 3, pp. 118–134, Aug. 2020.

[2] A. Khurram, H. Rehman, S. Mukhopadhyay, and D. Ali, "Comparative analysis of integer-order and fractional-order proportional integral speed controllers for induction motor drive systems," *J. Power. Electron.*, vol. 18, no. 3, pp. 723–735, 2018.

[3] A. K. Peter, J. Mathew, and K. Gopakumar, "A simplified DTC-SVPWM scheme for induction motor drives using a single PI controller," *IEEE Trans. Power Electron.*, vol. 38, no. 1, pp. 750–761, Jan. 2023.

[4] D. Giribabu, S. P. Srivastava, and M. K. Pathak, "Modified reference model for rotor flux-based MRAS speed observer using neural network controller," *IETE J. Res.*, vol. 65, no. 1, pp. 80–95, Jan. 2019, doi: 10.1080/03772063.2017.1407267.

[5] A. Rodriguez-Martinez and R. Garduno-Ramirez, "Comparative analysis of PI controller gain-scheduling through fuzzy systems," in *Proc. Electron., Robot. Automot. Mech. Conf. (CERMA)*, Sep. 2009, pp. 366–371.

[6] C. C. Lee, "Fuzzy logic in control systems: Fuzzy logic controller. I," *IEEE Trans. Syst., Man, Cybern.*, vol. 20, no. 2, pp. 404–418, Mar. 1990.

[7] M. N. Uddin, Z. R. Huang, and A. B. M. S. Hossain, "Development and implementation of a simplified self-tuned neuro–fuzzy-based IM drive," *IEEE Trans. Ind. Appl.*, vol. 50, no. 1, pp. 51–59, Jan. 2014.

[8] M. N. Uddin and H. Wen, "Development of a self-tuned neuro-fuzzy controller for induction motor drives," in *Proc. Conf. Rec. IEEE Ind. Appl. Conf., 39th IAS Annu. Meeting*, vol. 4, Seattle, WA, USA, Oct. 2004, pp. 2630–2636.

[9] W. Seok Oh, S. Kim, K. Min Cho, K. Sang Yoo, and Y. Tae Kim, "Genetic based self tuning speed controller for induction motor drives," in *Proc. Int. Conf. Appl. Supercond. Electromagn. Devices*, Sydney, NSW, Australia, Dec. 2011, pp. 88–91.

[10] Z. Ximei and S. Xianfeng, "Neural-network-based self-tuning PI controller for permanent magnet synchronous motor," in *Proc. Int. Conf. Electr. Mach. Syst.*, Beijing, China, Aug. 2011, pp. 1–4.

[11] J. Sun and W. Lin, "Non-identifier based adaptive regulation of feedforward systems with nonlinear parametrization and delays: A saturation control scheme," *Syst. Control Lett.*, vol. 173, Mar. 2023, Art. no. 105456. [Online]. Available: https://www.sciencedirect.com/science/article/pii/S0167691123000038

[12] I. Peter and S. John, *Robust Adaptive Control*. New York, NY, USA: Dover, 1996.

[13] S.-H. Chang and P.-Y. Chen, "Self-tuning gains of PI controllers for current control in a PMSM," in *Proc. 5th IEEE Conf. Ind. Electron. Appl.*, Taiwan, Jun. 2010, pp. 1282–1286.

[14] J. Park, H. Kim, K. Hwang, and S. Lim, "Deep reinforcement learning based dynamic proportional-integral (PI) gain auto-tuning method for a robot driver system," *IEEE Access*, vol. 10, pp. 31043–31057, 2022.

[15] E. Chavero-Navarrete, M. Trejo-Perea, J.-C. Jáuregui-Correa, R.-V. Carrillo-Serrano, and J.-G. Rios-Moreno, "Pitch angle optimization by intelligent adjusting the gains of a PI controller for small wind turbines in areas with drastic wind speed changes," *Sustainability*, vol. 11, no. 23, p. 6670, Nov. 2019, doi: 10.3390/su11236670.

[16] B. Kiyyour, L. Laggoun, A. Salhi, D. Naimi, and G. Boukhalfa, "Improvement DTC for induction motor drives using modern speed controllers tuning by PSO algorithm," *Periodica Polytechnica Electr. Eng. Comput. Sci.*, vol. 67, no. 3, pp. 249–259, Jul. 2023.

[17] R. Poola and T. Hanamoto, "Automated QFT-based PI tuning for speed control of SynRM drive with analytical selection of QFT control specifications," *Energies*, vol. 15, no. 2, p. 642, Jan. 2022.

[18] N. Pham and T. Le, "A novel FOC vector control structure using RBF tuning PI and SM for SPIM drives," *Int. J. Intell. Eng. Syst.*, vol. 13, no. 5, pp. 429–440, Oct. 2020.

[19] A. Wadi, S. Mukhopadhyay, and J.-H. Lee, "A novel disturbance-robust adaptive trajectory tracking controller for a class of underactuated autonomous underwater vehicles," *Ocean Eng.*, vol. 189, Oct. 2019, Art. no. 106377.

[20] R. Michino, H. Tanaka, and I. Mizumoto, "Application of high gain adaptive output feedback control to a magnetic levitation system," in *Proc. ICCAS-SICE*, Fukuoka, Japan, Aug. 2009, pp. 970–975.

[21] E. I. Al Khatib, W. M. F. Al-Masri, S. Mukhopadhyay, M. A. Jaradat, and M. Abdel-Hafez, "A comparison of adaptive trajectory tracking controllers for wheeled mobile robots," in *Proc. 10th Int. Symp. Mechatronics Appl. (ISMA)*, Dec. 2015, pp. 1–6.

[22] J. W. Polderman and I. M. Y. Mareels, "High gain adaptive control revisited: First and second order case," in *Proc. 38th IEEE Conf. Decis. Control*, vol. 4, Dec. 1999, pp. 3329–3333.

[23] F. Allgöwer, J. Ashman, and A. Ilchmann, "High-gain adaptive λ-tracking for nonlinear systems," *Automatica*, vol. 33, no. 5, pp. 881–888, May 1997.

[24] K. Narendra and A. Annaswamy, "A new adaptive law for robust adaptation without persistent excitation," *IEEE Trans. Autom. Control*, vol. AC-32, no. 2, pp. 134–145, Feb. 1987.

[25] N. T. Nguyen, "Optimal control modification for robust adaptive control with large adaptive gain," *Syst. Control Lett.*, vol. 61, no. 4, pp. 485–494, Apr. 2012.

[26] F. Blanchini, T. Parisini, F. A. Pellegrino, and G. Pin, "High-gain adaptive control: A derivative-based approach," *IEEE Trans. Autom. Control*, vol. 54, no. 9, pp. 2164–2169, Sep. 2009.

[27] M. P. R. V. Rao and T. J. Leckie, "Robust adaptive control: Improved e-modification," *IFAC Proc. Volumes*, vol. 31, no. 22, pp. 127–132, Aug. 1998.

[28] D. Jain and D. Saxena, "Comprehensive review on control schemes and stability investigation of hybrid AC–DC microgrid," *Electric Power Syst. Res.*, vol. 218, May 2023, Art. no. 109182. [Online]. Available: https://www.sciencedirect.com/science/article/pii/S0378779623000718

[29] H. M. Usman, H. Rehman, and S. Mukhopadhyay, "Electric vehicle traction system performance enhancement using FO-PI controller," in *Proc. IEEE Vehicle Power Propuls. Conf. (VPPC)*, Chicago, IL, USA, Aug. 2018, pp. 1–5.

[30] D. Matic, V. Bugarski, F. Kulic, and B. Dumnic, "Minimal configuration PI fuzzy gain scheduling speed controller in indirect vector controls scheme," in *Proc. 5th IET Int. Conf. Power Electron., Mach. Drives (PEMD)*, Brighton, U.K., 2010, pp. 1–6.

[31] R. Rodriguez, A. Fernando, A. C. Chavarro, M. Angel, T. Cardozo, J. Bernardo, J. R. Zarta, R. Serrezuela, A. Chavarro, M. Tovar, and J. Ramirez, "An optimal control based approach to dynamics autonomous vehicle," *Int. J. Appl. Eng. Res.*, vol. 10, pp. 235–249, May 2016.

[32] C. J. Stephen, *Electric Machinery Fundamentals*. New York, NY, USA: McGraw-Hill, 2012.

[33] P. C. Krause, O. Wasynczuk, S. D. Sudhoff, and S. Pekarek, *Analysis of Electric Machinery and Drive Systems*, vol. 2. Hoboken, NJ, USA: Wiley, 2002.

[34] M. A. Hannan, Md. M. Hoque, A. Hussain, Y. Yusof, and P. J. Ker, "State-of-the-art and energy management system of lithium-ion batteries in electric vehicle applications: Issues and recommendations," *IEEE Access*, vol. 6, pp. 19362–19378, 2018.

[35] L. Lu, X. Han, J. Li, J. Hua, and M. Ouyang, "A review on the key issues for lithium-ion battery management in electric vehicles," *J. Power Sources*, vol. 226, pp. 272–288, Mar. 2013.

SARAH ADNAN ALBARRI received the bachelor's and master's degrees in electrical engineering from American University of Sharjah (AUS) and the master's degree in machine learning from the Mohamed Bin Zayed University of Artificial Intelligence. Driven by interest in the cutting-edge field of artificial intelligence (AI). Currently, she is an Applied Natural Language Processing Scientist with Core42, a subsidiary of G42 Company.

AHMED KHALIL received the bachelor's and master's degrees in mechanical and mechatronics engineering from American University of Sharjah (AUS). He is currently pursuing Ph.D. degree in mechanical engineering with Texas A&M University, College Station, TX, USA. His affiliation with Texas A&M University involves focusing on metal 3D printing, machine learning, and control systems as part of his doctoral research. His research interests include model reference adaptive control (MRAC) systems, drones, mobile robots, and 3D printing. He has been awarded a Research Impact Initiative funding to pursue the Ph.D. degree.

SHAYOK MUKHOPADHYAY (Senior Member, IEEE) received the Ph.D. degree in electrical engineering from Georgia Institute of Technology, Atlanta, GA, USA, in 2014. Following this, he was with the Department of Electrical Engineering, American University of Sharjah, Sharjah, United Arab Emirates (UAE), until August 2023. Subsequently, he is with the ECECS Department, University of New Haven, West Haven, CT, USA. His research interests include robotics and automation, control systems, nonlinear systems, mechatronics, renewable energy systems, computational methods, battery modeling and failure detection, and robotic path planning. He was a recipient of the Award for the Best Presentation in the Nonlinear Systems III Session from American Control Conference, in 2014. He was a part of a five-person team that received the national category of UAE, AI and Robotics for Good Awards, in 2017, for developing an in-pipe inspection robot. He also served as the Chair for IEEE UAE Section CSS/RAS/EMBS Joint Chapter, from 2022 to 2023.

HABIBUR REHMAN (Member, IEEE) received the B.Sc. degree in electrical engineering from the University of Engineering and Technology, Lahore (UET Lahore), Pakistan, in 1990, and the M.S. and Ph.D. degrees in electrical engineering from The Ohio State University, Columbus, OH, USA, in 1995 and 2001, respectively. He has wide experience in the areas of power electronics, motor drives, and power systems in both industry and academia. From 1998 to 1999, he was a Design Engineer with the Ecostar Electric Drive Systems and Ford Research Laboratory, where he was a member of the Electric, Hybrid, and Fuel Cell Vehicle Development Programs. From 2001 to 2006, he was with the Department of Electrical Engineering, United Arab Emirates University, Al Ain, United Arab Emirates, as an Assistant Professor. In 2006, he joined the Department of Electrical Engineering, American University of Sharjah, where he is currently a Professor. His primary research interests include power electronics and their application to power systems, adjustable-speed drives, and alternative energy vehicles.